JTTEE5 18:201–208
DOI: 10.1007/s11666-009-9313-6
1059-9630/$19.00 © ASM International

Effect of Thermal Aging on Microstructure and Functional Properties of Zirconia-Base Thermal Barrier Coatings

N. Markocsan, P. Nylén, J. Wigren, X.-H. Li, and A. Tricoire

(Submitted November 7, 2008; in revised form February 16, 2009)

Thermal barrier coating (TBCs) systems made of plasma sprayed zirconia are commonly used in gas turbine engines to lower metal components surface temperature and allow higher combustion temperature that results in higher fuel efficiency and environmentally cleaner emissions. Low thermal conductivity and long service life are the most important properties of these coatings. The objective of this work was to study the influence of a long-term heat treatment (i.e., 1200 °C/2000 h) on different characteristics of atmospheric plasma sprayed TBCs. Two zirconia feedstock materials were evaluated, namely, yttria partially stabilized zirconia and dysprosia partially stabilized zirconia. Several spray conditions were designed and employed to achieve different coating morphologies. Microstructure analyses revealed that the coating microstructure was significantly dependent on both operating conditions and heat treatment conditions. Significant changes in coatings porosity occurred during heat treatment. The lowest thermal conductivity was reached with the dysprosia partially stabilized zirconia material. Heat treatment affected TBCs adhesion strength as well.

Keywords heat treatment, plasma spray, porosity, TBCs, thermal conductivity, zirconia

1. Introduction

Thermal spray coatings are currently used for different applications in a variety of industries such as automotive, aerospace, and biomedical (Ref 1). Thermal barrier coating (TBC) systems are among the most predominant thermal spray applications and are designed to protect hot section components in gas turbines or automotive engines (Ref 2). Important efforts have been devoted in the last decades to improve TBC performance (Ref 3, 4). An evidence of the complexity as well as of the interest for this topic is reflected by the high number of publications and research projects as well as seminars and conferences dedicated to TBCs. A significant number of reviews on different aspects of TBCs can be found in the recent literature (Ref 2, 5-10).

A TBC consists typically of two layers, a metallic layer called bondcoat and a ceramic layer called topcoat. The bondcoat improves the bonding strength of the topcoat and protects the substrate from corrosion and oxidation, whereas the topcoat protects the substrate from thermal degradation and reduces the service temperature. An early investigation done by Stecura (Ref 11) more than 20 years ago, showed that the best thermal cycling performance among atmospheric plasma sprayed (APS) topcoat materials was shown to be the 6 to 8 wt.% yttria stabilized zirconia (6-8YPSZ) material with an optimal porosity of 14 to 15 vol.%. Nowadays, the 6-8YPSZ coatings, deposited either by APS or by electron beam physical vapor deposition (EB-PVD), are still the most frequently used in gas turbine applications (Ref 2, 5, 12). As demands of higher operating temperatures and/or longer service times increase, new materials have to be found. In a TBC system, detrimental changes occur during service as a result of both high thermal and mechanical loads. Under these loading conditions, the components of the coating system—that is, substrate, bondcoat, and topcoat—react and interact in different ways with the environment or/and with each other. The functional performance and durability of a TBC system are influenced by numerous factors such as thermal expansion mismatch between the ceramic layer and the metal substrate, thermal stresses generated by the temperature gradients in the TBC, topcoat sintering, phase transformations, corrosive and erosive environment, residual stresses arising from the deposition process, bondcoat oxidation, development of thermally grown oxides (TGO), calcium-magnesium aluminosilicate (CMAS) infiltration, and long-term stability (Ref 13-17). Development of coating materials and deposition methods is thus a challenging issue for both industry and academia.

Many research studies have been devoted to evaluation of TBC systems behavior and properties during and after short-term heat treatment (i.e., <100 h) (Ref 18-21), but very limited studies have been conducted during or after long-term thermal exposure (i.e., >1500 h).

N. Markocsan and **P. Nylén**, University West, Trollhättan, Sweden; **P. Nylén, J. Wigren,** and **A. Tricoire**, Volvo Aero Corporation, Trollhättan, Sweden; and **X.-H. Li**, Siemens Industrial Turbomachinery AB, Finspång, Sweden. Contact e-mail: nicolaie.markocsan@hv.se.

The objective of this study was thus to study the influence of a long-term heat treatment (i.e., 1200 °C/2000 h) on different coating characteristics of atmospheric plasma sprayed TBC systems.

2. Experimental Methods and Materials

2.1 Materials and Specimen Preparation

Two different substrate geometries of Hastelloy X specimens were used, square plates (25 × 25 × 1.5 mm) and cylindrical coupons (∅25 × 6.35 mm). Prior to being coated, the substrates were cleaned with acetone and then grit blasted with grit 60 alumina grit using a pressure of 4 bar. The coatings were atmospheric plasma sprayed using the A3000S Sulzer Metco spray system equipped with a F4 gun (Plasma-Technik A3000S, Sulzer Metco AG, Wohlen, Switzerland).

The 100 to 150 μm thick bondcoat was sprayed using a commercial NiCoCrAlY powder (AMDRY 365-2). Three zirconia-base powders were sprayed 300 to 450 μm in thickness. The topcoat powder compositions and morphologies are presented in Table 1.

Three spraying regimes were developed to spray the topcoat materials: SR1, high power and medium feed rate; SR2, high power and high feed rate; and SR3, low power and low feed rate. Seven different coating systems were sprayed, as listed in Table 2. More details about spray conditions and operating parameters for spraying of bondcoat and topcoat materials can be found in Ref 22.

Two samples (i.e., A&S 7YPSZ SR1-b and HOSP 8YPSZ SR3-b) were sprayed after a period of 10 months, using the same operating parameters. The main purpose for spraying these samples was to evaluate the influence of process reproducibility on coating properties.

2.2 Microstructure and Porosity Evaluation

Microstructure cross-section evaluations of coatings were carried out using both optical microscopy (OM) and scanning electron microscopy (SEM). In order to evaluate coating porosity, an image analysis procedure was employed (referred to as Routine IA) that previously had been developed within a Brite Euram Project (Ref 23). More details about this procedure can be found in Ref 24. As shown in a previous work (Ref 22), for a more accurate porosity evaluation, the pores were divided in cracks and globular pores. The distinguishing factor was the area/perimeter ratio (circularity) of each analyzed feature; it was considered a crack if circularity was between 0 and 0.8, and considered a globular pore if circularity was greater than or equal to 0.8 and less than or equal to 1. For each sample, analysis was performed on 25 distinct areas of the cross section. The area covered by each OM micrograph was 429 × 343 mm. The standard deviation of the image analysis method was 0.3%.

Table 1 Feedstock characteristics of the zirconia powders

Symbol/Manufacturer	Composition, wt.%	Powder morphology	Particle size, μm
7YPSZ/H.C. Starck	ZrO_2-7Y_2O_3	A&S(a)	−90 +20
8YPSZ/Sulzer Metco	ZrO_2-8Y_2O_3	HOSP(b)	−75 +20
4DyPSZ/Sulzer Metco	ZrO_2-4 mol.% Dy_2O_3	HOSP(b)	−90 +20

(a) Agglomerated and sintered, (b) Homogenized oven spheroidized particles

2.3 Heat Treatment

Prior to thermal conductivity determination, the samples were exposed for 2 h at 1150 °C, in atmospheric conditions, in order to minimize the transient microstructure change with temperature. This heat treatment is hereafter referred to as short heat treatment (S-HT).

Long-term heat treatment (L-HT) was performed using the temperature-time schedule shown in Fig. 1. The L-HT was carried out in an oven under normal atmospheric conditions.

2.4 Thermal Conductivity Determination

Coatings thermal diffusivity was measured by the Laser Flash technique using the finite pulse duration method (Ref 25, 26). The heat pulse was supplied by a solid-state Nd-glass laser ($\lambda = 1.067$ μm) with a beam diameter of 16 mm. The energy output was in the range 5 to 95 J, and the pulse dissipation time 0.6 ms. The pulse profile was determined and the finite pulse time effects were corrected using the method developed by Clark and Taylor (Ref 27). The temperature rise of the opposite face was monitored by an In-Sb infrared detector, sensitive to 5.5 μm and having a response time of 1.5 μs. Heat losses were corrected using the method developed by Cowan (Ref 28). The accuracy of the measurement method was in the range of ±5%.

A disk-shaped free-standing ceramic sample with a diameter of 10 mm and thickness of 300 to 450 μm was used in these measurements. The samples were coated with a thin layer of carbon before the measurements in order to prevent reflection and transmittance of the laser pulse. The measurements were done in argon at or slightly above atmospheric pressure.

Table 2 Coating specimens and operating parameters

Coating specimen	Powder	Arc power, kW	Powder feed rate, g/min	Spraying regime
A&S 7YPSZ SR1-a	A&S 7YPSZ	44.8	90	SR1
A&S 7YPSZ SR2		44.8	180	SR2
A&S 7YPSZ SR3		38.5	40	SR3
A&S 7YPSZ SR1-b(a)		44.8	90	SR1
HOSP 8YPSZ SR3-a	HOSP 8YPSZ	38.5	40	SR3
HOSP 8YPSZ SR3-b(a)		38.5	40	SR3
HOSP 4DyPSZ SR1	HOSP 4DyPSZ	44.8	90	SR1
HOSP 4DyPSZ SR2		44.8	180	SR2
HOSP 4DyPSZ SR3		38.5	40	SR3

(a) Process reproducibility test samples

Measurements were recorded from room temperature up to 1000 °C, at intervals of approximately 100 °C.

At least 10 measurements were recorded at each temperature interval, and an average value calculated.

The thermal conductivity was calculated using:

$$k = \alpha C_p \rho$$

where k denotes the thermal conductivity, α the thermal diffusivity, C_p the specific heat, and ρ is the density of the coatings.

C_p values for each measurement temperature were determined by calculation, using literature data, for the YPSZ coatings (Ref 29, 30) and by differential scanning calorimetry, for the DyPSZ coatings (Ref 23, 31). Average density values were determined using the Archimedes method to 5.058 g/cm^3 for YPSZ and to 5.12 g/cm^3 for DyPSZ.

2.5 Adhesion Tensile Strength Evaluation

The standard ASTM C 633 tensile test was carried out to measure the adhesion strength of the zirconia coatings. An F1000 type adhesive agent was used to join the test specimens (1 in. in diameter) with the cylindrical counter parts. After being cured at elevated temperature, a tensile load was applied using a universal tensile test machine. The mean adhesive strength values were calculated from testing at least three specimens having topcoats deposited under the same spraying conditions.

Three sets of coatings were used for adhesion testing: as-sprayed, heat treated at 800 °C for 2 h, and heat treated at 1150 °C for 2 h. No adhesion test was performed on the samples after the L-HT since the coating surfaces lost their planarity; hence gluing the samples to their counterparts was not possible.

3. Results and Discussion

3.1 Microstructure

Examples of microstructure images of sprayed coatings are presented in Fig. 2 and 3. As expected, the as-sprayed coatings (Fig. 2) revealed a predominantly lamellar

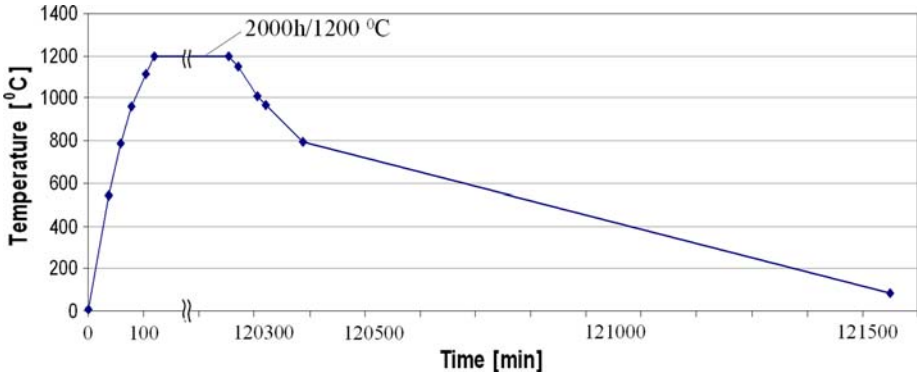

Fig. 1 Diagram of the long heat treatment

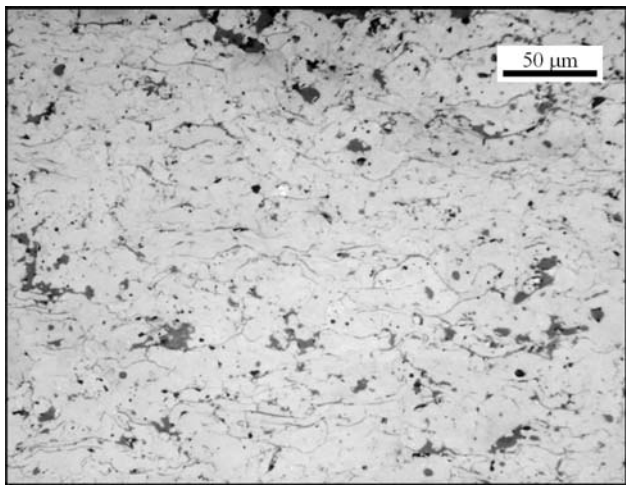

Fig. 2 HOSP 4DyPSZ SR1, as-sprayed

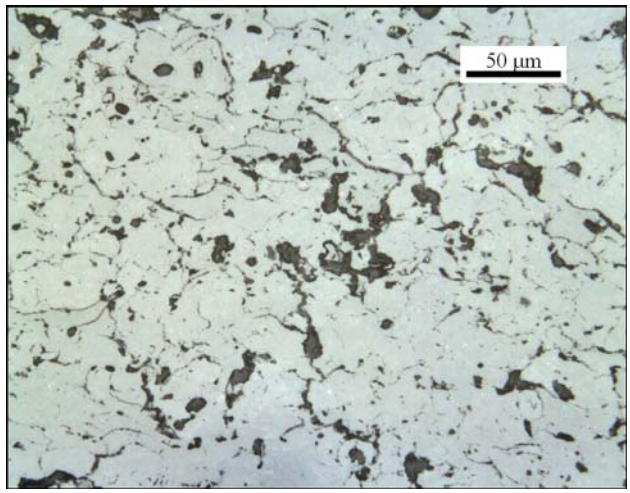

Fig. 3 HOSP 4DyPSZ SR1, after long heat treatment

structure with a rather low amount of unmolten particles. The degree of the unmolten particles was found to be more dependent on spray parameters than on powder morphology or chemistry. Mainly two predominantly types of pores were observed: globular pores and fine horizontal intersplat cracks (also called delaminations). Both globular pores and cracks were uniformly distributed through the coating.

Changes were observed in the coatings microstructure after the L-HT (Fig. 3). A first observation was a higher amount of globular pores. They were rather more numerous than bigger in size and predominantly interconnected and/or grouped in clusters. A second observation was that the fine horizontal intersplat cracks almost disappeared and ''replaced'' with fewer but larger cracks, after the heat treatment. The orientation of the large cracks was found to be more aleatory (slightly vertically) compared with delaminations in the as-sprayed coatings that were mostly horizontally oriented. An explanation for these microstructural changes can be the significant sintering that occurred in coatings during L-HT. During this rather long solid-state sintering process, first the small-scale voids (of nanometric size) and small delaminations (splat boundaries) sintered; then the existing pores (too large to sinter) reconfigured, based on minimal energy effects, that is, smaller delaminations (splat boundaries), large enough not to fuse, became spherical for minimal energy reasons. The solid-state sintering process caused an increase of coatings stiffness as well as coating shrinkage, which in turn led to higher local residual stress up to a level from which new cracks were initiated (rather vertically oriented) and also probably acted on the unsintered pores enlarging them.

3.2 Porosity

Figure 4 shows the total porosity (in vol.%) of the coatings, as-sprayed, after S-HT and after L-HT.

Insignificant changes were found in the coating porosity after the S-HT (2 h/1150 °C); the total porosity of all analyzed coatings in general decreased slightly (Fig. 4). This reduction can be attributed to the solid-state sintering during the heat treatment that acted mostly on small cracks and voids. More significant changes occurred in coatings porosity after the L-HT. The total porosity in all investigated coatings varied in a narrower range after the L-HT (i.e., 15.7 to 22.2%) compared with the as-sprayed coatings where it varied between 9.0 and 21.3%.

Figures 5 and 6 present the crack evolution during heat treatments and globular pores during heat treatments, respectively.

No significant changes of the total volume of the cracks were observed in coatings after L-HT (Fig. 5). As commented previously, during the L-HT the high number of fine horizontal cracks was replaced with fewer and larger cracks. However, this reconfiguration of the cracks morphology occurred with insignificant changes in total volume of the cracks.

Globular pores showed a much differentiated variation after the L-HT (Fig. 6). In three coatings [i.e., A&S 7YPSZ SR2, A&S 7YPSZ SR3, and HOSP 8YPSZ SR3(a)], the volume of globular pores was almost constant thorough all heat treatments, whereas in the rest of the coatings significant variation occurred after the L-HT. It can be worth noting that all coatings that underwent high variations of globular pores during the L-HT possessed the lowest amount of globular pores in the as-sprayed state (approximately 8 vol.% or lower), whereas those three coatings with higher amounts of globular pores before L-HT showed almost no changes after the L-HT. More experiments are needed to understand all mechanisms and phenomena behind these results such as why the porosity of some coatings changed a lot, while the porosity of other coatings did not change or even decreased. Apart from the fusing effect discussed previously, other mechanisms could concur independently or interdependently to porosity change during and/or after L-HT. Examples are (a) more pullouts during sample preparation (i.e., less effect of the vacuum impregnation because

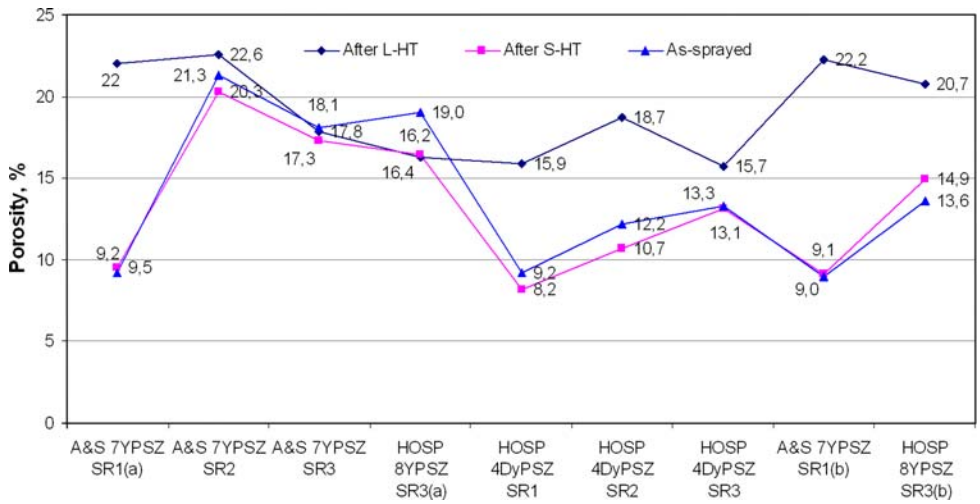

Fig. 4 Evolution of the total porosity in TBCs, after different treatments

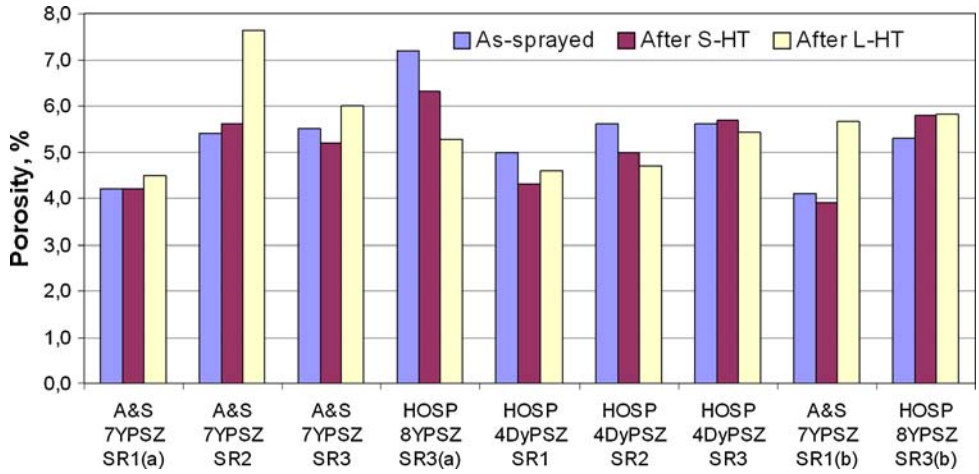

Fig. 5 Cracks evolution during heat treatments

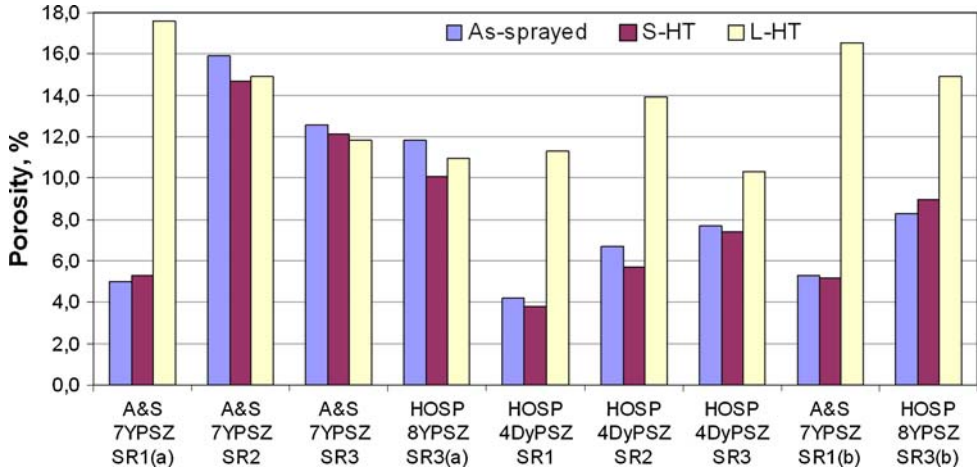

Fig. 6 Globular pore evolution during heat treatments

of the brittleness of the topcoat after L-HT), (b) volume changes caused by phase transformations during and after heat treatment, (c) not the same temperature reached the samples during L-HT (i.e., all samples were annealed together in an oven, and thus there could have been local temperature differences at different locations), (d) errors induced by the porosity measurement software (i.e., in the as-sprayed state, the very fine cracks and pores could have been rejected), (e) powders different impurities content of powders.

3.3 Thermal Conductivity

Measured thermal diffusivity values of the coatings are shown in Fig. 7 and calculated thermal conductivity values in Fig. 8.

As one can see in Fig. 7, the thermal diffusivity decreased with temperature. Despite the similar trend of the thermal diffusivity curves, different individual values were measured on the coatings. These differences came mainly from the differences in coating microstructure and/or chemistry.

The majority of the investigated TBC systems showed, up to a temperature of 300 to 400 °C, a decrease of thermal conductivity with temperature (Fig. 8). From this interval to higher temperatures the thermal conductivity was almost constant, with small oscillations up and down that corresponded to different temperatures and hence to different phenomena and thermal transport mechanisms.

A comparison between the thermal conductivity values before and after the L-HT is presented in Fig. 9. The coatings after L-HT are represented with filled symbols. Corresponding total porosity values of coatings are plotted as well.

The calculated thermal conductivity values were in the range of 1.7 to 2.7 and 1.5 to 1.8 W/m °C at room temperature and 1000 °C, respectively. If these results are compared with those found on the same coatings before L-HT (i.e., 0.9-1.2 and 0.7-1.1 W/m °C at room temperature and 1000 °C, respectively), it can be observed that

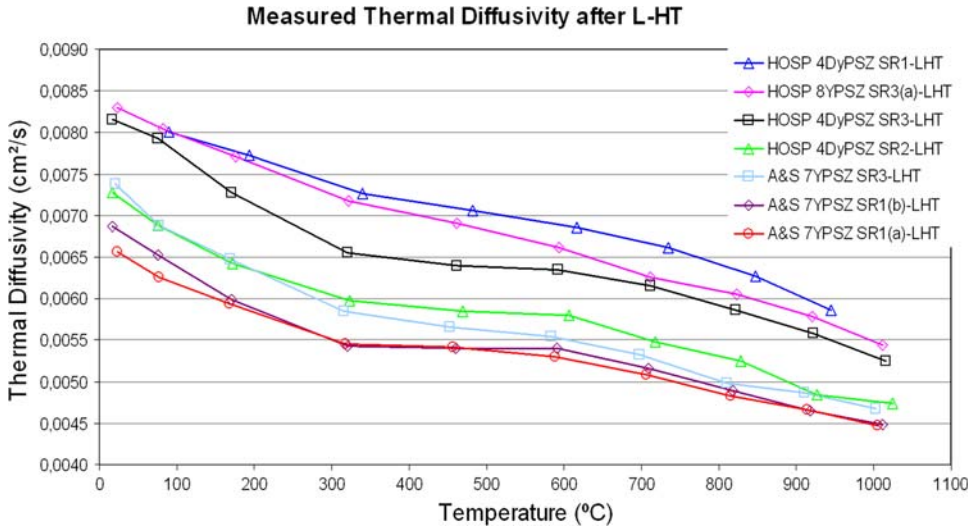

Fig. 7 Measured thermal diffusivity, 20-1000 °C temperature range

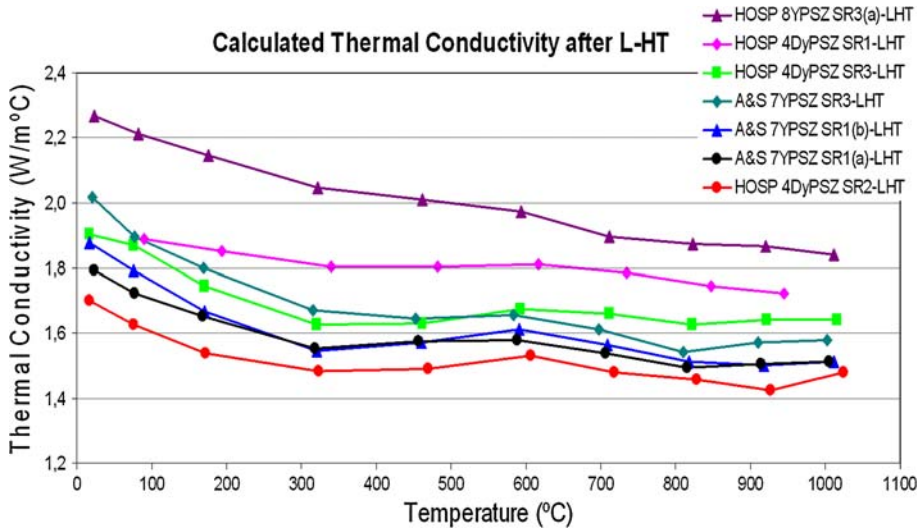

Fig. 8 Calculated thermal conductivity, 20-1000 °C temperature range

coatings thermal conductivity raised after L-HT, in average, with almost 1 W/m °C. This increase of thermal conductivity was surprising as the porosity values increased in a majority of the coatings after the L-HT as well. Some possible explanations to this discrepancy are: (a) under the L-HT the small-scale porosity was drastically reduced (as shown previously), and hence the sintered coatings missing this kind of porosity show higher thermal conductivity (this result may confirm the high importance of the small (nano-) scale porosity on thermal transport properties of TBC systems); (b) the new phases that appeared during L-HT have higher conductivity (i.e., higher amounts of monoclinic); (c) it is known that thermal conductivity does not really correlate to globular pores, but rather to delaminations or ''flat'' elongated pores; therefore, as the fine horizontal intersplat cracks were reduced significantly and replaced with aleatory oriented cracks, coatings revealed diminished thermal isolation properties.

The lowest thermal conductivity after L-HT was reached with one of the DyPSZ coatings. Within the entire interval of the investigated temperatures, the HOSP 4DyPSZ SR2 coating showed the lowest thermal conductivity despite its lower porosity (i.e., 18.7%) compared with the coating with the closest thermal conductivity (i.e., A&S 7YPSZ SR1-a) but higher porosity (i.e., 22%).

The other coatings made of HOSP powders showed higher thermal conductivity than those made of A&S powder, but their porosity was also lower than of those sprayed with A&S powder.

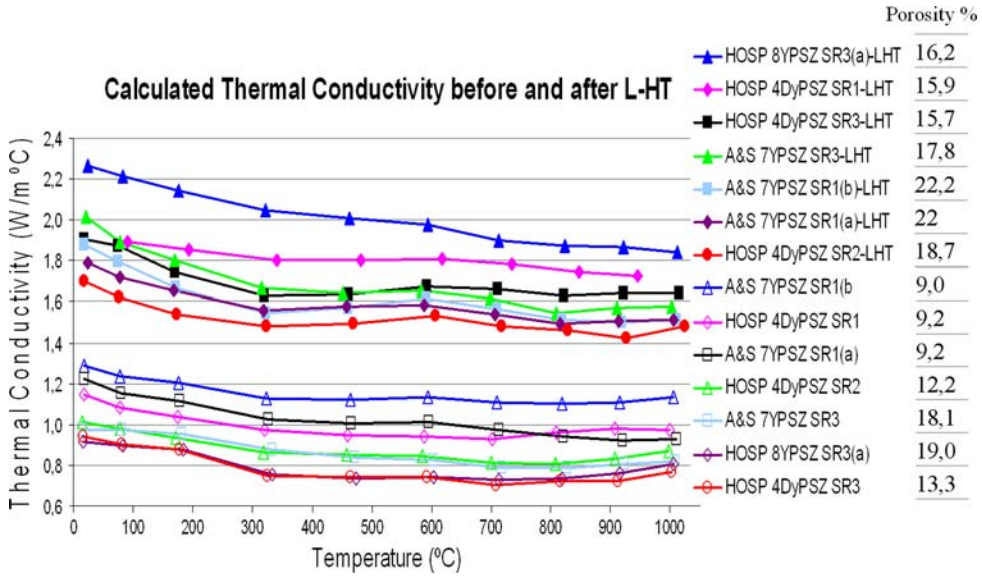

Fig. 9 TBCs thermal conductivity, before and after L-HT

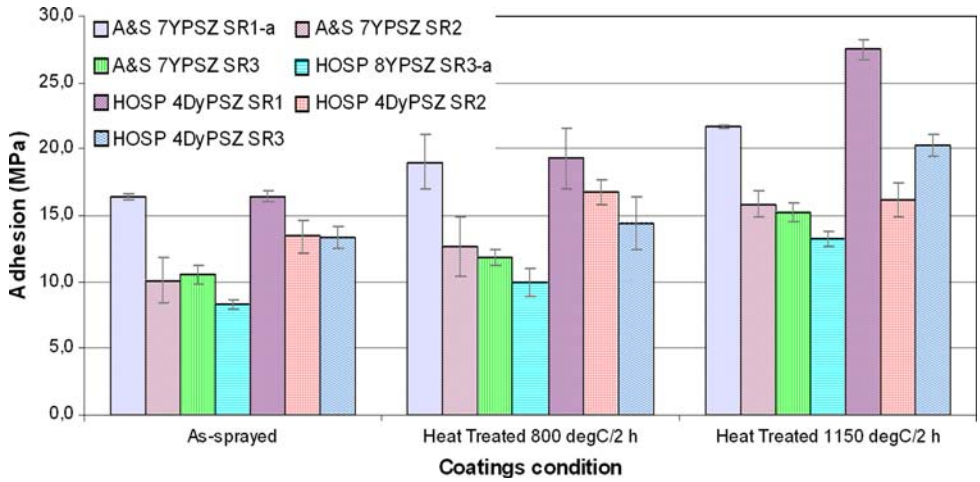

Fig. 10 Measured adhesion strength values of coatings

3.4 Adhesion

The measured adhesion strength values of the coatings after different treatments are shown in Fig. 10.

All tested specimens showed a failure mode located at the interface between topcoat and bondcoat. The highest strength adhesion values were reached with both YPSZ and DyPSZ coatings sprayed with high-energy plasma (i.e., SR1), whereas all coatings sprayed with SR2 and SR3 spray regimes revealed lower values. All three DyPSZ coatings showed higher or at least equal adhesion strength values compared with the YPSZ coatings sprayed with similar spray parameters. It has to be noted that heat treatment affected the adhesion strength of the topcoats. All TBCs revealed an increase of their adhesion strength after both heat treatments (i.e., 800 °C/2 h and 1150 °C/2 h), and moreover the adhesion strength increased with the heat treatment temperature. A possible reason for the higher adhesion strength values after the heat treatments could be the thin and adherent oxide layer that usually develops at the interface between topcoat and bond layer during heat treatments carried out in air. More investigations are to be carried out to better understand and find out all correlations that exist between the heat treatment conditions and the adhesion strength of the coatings.

4. Conclusions

The influence of a long heat treatment (2000 h/1200 °C) on different coating characteristics of two types of TBC systems (i.e., YPSZ and DyPSZ) was analyzed in this work. The microstructure analysis revealed that

coating microstructure was significantly dependent on both spraying parameters and heat treatment conditions. Significant changes in coating porosity occurred under the long heat treatment. Powder composition is as influential as coating porosity or powder morphology on TBCs heat conductivity. The lowest thermal conductivity of the coatings after long heat treatment, measured within the entire interval of investigated temperatures, was reached with the DyPSZ coatings (in conditions of same or lower porosity than those of the other investigated coatings). All TBCs showed higher adhesion strength after short heat treatments (i.e., 800 °C/2 h and 1150 °C/2 h).

References

1. J.R. Davis, Ed., *Handbook of Thermal Spray Technology*, ASM International, Materials Park, OH, 2004
2. R.A. Miller, Thermal Barrier Coatings for Aircraft Engines: History and Directions, *J. Therm. Spray. Technol.*, 1997, **6**(1), p 35-42
3. J.R. Nicholls, Advances in Coating Design for High Performance Gas Turbines, *MRS Bull.*, 2003, **28**(a), p 659-670
4. W.A. Nelson and R.M. Orenstein, TBC Experience in Land/Based Gas Turbines, *J. Therm. Spray. Technol.*, 1997, **6**(2), p 176-180
5. S.M. Meier and D.K. Gupta, The Evolution of Thermal Barrier Coatings in Gas Turbine Engine Applications, *Trans. ASME*, 1994, **116**, p 250-256
6. C.G. Levi, Emerging Materials and Processes for Thermal Barrier Systems, *Curr. Opin. Solid State Mater. Sci.*, 2004, **8**, p 77-91
7. R. Vaßen, F. Cernuschi, G. Rizzi, N. Markocsan, L. Östergren, A. Kloosterman, R. Mevrel, J. Feist, and J. Nicholls, Overview in the Field of Thermal Barrier Coatings Including Burner Rig Testing in the European Union, *Bull. Ceram. Soc. Jpn.*, 2008, **43**, p 371-383
8. U. Schulz, C. Leyens, K. Fritscher, M. Peters, B. Saruhan-Brings, and O. Lavigne, Some Recent Trends in Research and Technology of Advanced Thermal Barrier Coatings, *Aerospace Sci. Technol.*, 2003, **7**, p 73-80
9. J. Wigren and L. Pejryd, Thermal Barrier Coatings—Why, How, Where and Where to, *Proceedings of the 15th International Thermal Spray Conference—Thermal Spray: Meeting the Challenges of the 21st Century,* C. Coddet, Ed., May 25-29, 1998 (Nice, France), ASM International, 1998, p 1531-1542
10. N.P. Padture, M. Gell, and E.H. Jordan, Thermal Barrier Coatings for Gas Turbine Engine Applications, *Science*, 2002, **296**, p 280-284
11. S. Stecura, Optimization of the Ni-Cr-Al-Y/ZrO_2-Y_2O_3 Thermal Barrier System, *Adv. Ceram. Mater.*, 1986, **1**(1), p 68-76
12. R. Vaßen and D. Stöver, Influence of Microstructure on the Thermal Cycling Performance of Thermal Barrier Coatings, *Proceedings of the Conference Thermal Spray 2007: Global Coating Solutions,* B.R. Marple, M.M. Hyland, Y.-C. Lau, C.-J. Li, R.S. Lima, and G. Montavon, Eds., ASM International, Materials Park, OH, 2007
13. C. Giolli, A. Scrivani, G. Rizzi, F. Borgioli, G. Bolelli, and L. Lusvarghi, Failure Mechanism for Thermal Fatigue of Thermal Barrier Coating Systems, *Proceedings of the International Thermal Spray Conference—Thermal Spray Crossing Borders,* ITSC 2008, E. Lugscheider, Ed., DVS-Verlag GmbH, Dusseldorf, Germany, 2008
14. J.A. Haynes, E.D. Rigney, M.K. Ferber, and W.D. Porter, Thermal Cycling Behaviour of Plasma-Sprayed Thermal Barrier Coatings with Various MCrAlY Bond Coats, *J. Therm. Spray Technol.*, 2000, **9**(1), p 38-48
15. P. Scardi, M. Leoni, and L. Bertamini, Influence of Phase Stability on the Residual Stress in Partially Stabilized Zirconia TBC Produced by Plasma Spray, *Surf. Coat. Technol.*, 1995, **76-77**, p 106-112
16. K.M. Grant, S. Krämer, J. Löfvander, and C. Levi, CMAS Degradation of Environmental Barrier Coatings, *Surf. Coat. Technol.*, 2007, **202**(4-7), p 653-657
17. A.G. Evans, D.R. Mumm, J.W. Hutchinson, G.H. Meier, and F.S. Pettit, Mechanisms Controlling the Durability of Thermal Barrier Coatings, *Progr. Mater. Sci.*, 2001, **46**, p 505-553
18. R.W. Trice, Y.J. Su, J.R. Mawdsley, K.T. Faber, A.R. De Arellano-López, H. Wang, and W.D. Porter, Effect of Heat Treatment on Phase Stability, Microstructure, and Thermal Conductivity of Plasma-Sprayed YSZ, *J. Mater. Sci.*, 2002, **37**, p 2359-2365
19. R.A. Miller, J.L. Smialek, and R.G. Garlick, Phase Stability in Plasma-Sprayed, Partially Stabilized Zirconia-Yttria, *Science and Technology of Zirconia, Advances in Ceramics,* Vol. 3., A.H. Heuer and L.W. Hobbs, Eds., The American Ceramic Society, 1981, p 241-253
20. J. Moon, H. Choi, H. Kim, and C. Lee, The Effects of the Heat Treatment on the Phase Transformation Behavior of Plasma-Sprayed Stabilized ZrO_2 Coatings, *Surf. Coat. Technol.*, 2002, **155**, p 1-10
21. J. Ilavsky and J.K. Stalick, Phase Composition and its Changes During Annealing of Plasma-Sprayed YSZ, *Surf. Coat. Technol.*, 2000, **127**, p 120-129
22. N. Markocsan, P. Nylen, J. Wigren, and X.-H. Li, Low Thermal Conductivity Coatings for Gas Turbine Applications, *J. Therm. Spray Technol.*, 2007, **16**(4), p 498-505
23. J. Wigren, High Insulation Thermal Barrier Systems—HITS, Brite Euram Project BE96-3226, 1996
24. O. Lavigne, Y. Renollet, M. Poulain, C. Rio, P. Moretto, P. Brannvall, and J. Wigren, Microstructural Characterization of Plasma Sprayed Thermal Barrier Coatings by Quantitative Image Analysis, Quantitative Microscopy of High Temperature Materials Conference, Sheffield, UK, 1999
25. W.J. Parker, R.J. Jenkins, C.P. Butler, and G.L. Abort, Flash Method of Determining Thermal Diffusivity, Heat Capacity, and Thermal Conductivity, *J. Appl. Phys.*, 1961, **32**, p 1679-1684
26. R. Taylor, Construction of Apparatus for Heat Pulse Thermal Diffusivity Measurements from 300-3000 K, *J. Phys. E Sci. Instrum.*, 1980, **13**, p 1193-1199
27. L.M. Clark and R.E. Taylor, Radiation Loss in the Flash Method for Thermal Diffusivity, *J. Appl. Phys.*, 1975, **46**(2), p 714-719
28. D. Cowan, Pulse Method of Measuring Thermal Diffusivity at High Temperatures, *J. Appl. Phys.*, 1963, **34**(4), p 926-927
29. R. Brandt, L. Pawlowski, and G. Neuer, Specific Heat and Thermal Conductivity of Plasma Sprayed Yttria-Stabilised Zirconia and NiAl, NiCr, NiCrAl, NiCrAlY, NiCoCrAlY Coatings, *High Temp.—High Pressures*, 1986, **18**, p 65-77
30. K.E. Wilkes and J.F. Lagedrost, Thermophysical Properties of Plasma Sprayed Coatings, Report NASA-CR-121144, National Aeronautics and Space Administration, 1973
31. J. Wigren, Improved Plasma Sprayed Thermal Barriers for Relevant Combustor Geometries Using Enhanced Process Control and Better Test Technologies-COMBCOAT, Brite Euram Project BRE-CT94-0936, 1994